Photoluminescent Properties of Tb-UiO-66 Metal–Organic Framework Analogues

Ximena A. Canales Gálvez,[a,‖] Micaela Richezzi,[a,‖] Hudson A. Bicalho,[a] Natalia Labadie,[b] Silvina C. Pellegrinet,[b] Hatem M. Titi,[c] Ashlee J. Howarth[*a]

[a]Department of Chemistry and Biochemistry and Centre for NanoScience Research, Concordia University, 7141 Sherbrooke Street West, Montreal, Quebec, H4B 1R6, Canada

[b]Instituto de Química Rosario (CONICET), Facultad de Ciencias Bioquímicas y Farmacéuticas, Universidad Nacional de Rosario, Suipacha 531, Rosario, Santa Fe, 2000, Argentina

[c]Department of Chemistry, McGill University, 801 Sherbrooke Street West, Montreal, Quebec, H3A 0B8, Canada

Rare-earth, MOFs, RE-MOFs, Lanthanoid, Photoluminescence, Terbium

ABSTRACT: Three new analogues of Tb-UiO-66 with various functional groups (–F, –Br, –NH_2) on the terephthalic acid linker of the metal–organic framework (MOF) are synthesized and characterized. The photoluminescent properties of these analogues, as well as Tb-UiO-66 and Tb-UiO-66-$(OH)_2$, are studied and correlated to the calculated energies for the triplet (T_1) states of each linker. The results show that the addition of electron withdrawing groups, such as –F and –Br, lead to higher T_1 energies, resulting in quantum yields in the range of 6-31 %. The addition of electron donating groups, on the other hand, lowers the T_1 energy of the organic linker and inhibits energy transfer such that emission is not observed.

1. INTRODUCTION

Over the past few decades, metal–organic frameworks (MOFs) have gathered considerable attention due to their potential for high surface area, crystallinity, and tunable chemical composition.[1, 2] These porous materials arise from the combination of inorganic building units with multitopic organic ligands.[3, 4] Due to their versatility, MOFs can be used for various applications ranging from gas storage[5] to catalysis,[6-8] amongst others.[9]

There are seventeen rare earth (RE) elements, including scandium, yttrium and the fifteen lanthanoids from the *f*-block of the periodic table. The lanthanoids have unique luminescent properties, including narrow emission peaks, large Stokes shifts, and long luminescent lifetimes which makes them an interesting choice for incorporation in materials for sensing,[10] bioimaging,[11] and light emitting diodes (LEDs).[12] Using lanthanoid ions in MOF metal nodes allows for the formation of porous materials that can be utilized for the optoelectronic applications previously mentioned, with the added benefit of high analyte adsorption,[13] drug encapsulation,[14] or the ability to incorporate photoactive guest molecules in the pores.[11] However, lanthanoid ions have low molar absorptivity (ε), leading to weak absorption and subsequently weak luminescence intensity when performing direct excitation into the metal *f-f* energy levels.[15] To overcome this limitation, lanthanoid ions are often paired with chromophores having high molar absorptivity to allow for photon absorption and subsequent energy transfer from the chromophore to the lanthanoid ions 4*f* excited states, improving the brightness of emission observed.[16-18] This process is also known as the "antenna effect".[19, 20]

In 2021, a library of RE analogues of UiO-66 was reported by our research group demonstrating crystallinity, thermal stability, and porosity.[21] In these MOFs, the RE ions form a hexanuclear cluster where the metal ions are bridged by a combination of μ_3-OH and μ_3-F ligands.[22] The use of fluorinated modulators is required for the synthesis of these RE_6-clusters, allowing for the incorporation of μ_3-F ligands in the structure.

Since 2021, our group has continued to explore the synthetic conditions required to obtain RE-UiO-66, showing that acetate precursors can be used instead of the traditional nitrates,[23] and that single crystals can be obtained under certain conditions.[24] These single crystals were used to study the correlation between the decomposition temperature of the material and the bond length between the metal and the linker.

Additionally, we observed strong photo- and radioluminescence in Tb-UiO-66.[25] This MOF displays green metal-based emission when excited at 355 nm into the terephthalic acid linker (BDC) and the reported results confirm that the antenna effect occurs in this MOF. We also showed that white light emission can be observed by tuning the metal composition of RE-UiO-66 in order to obtain a trimetallic Tb:Gd:Eu MOF, taking advantage of the photoluminescent properties of these metals.[26]

In this work, we explore the photoluminescent properties of Tb-UiO-66 analogues through varying the functional groups on the terephthalic acid linker in order to modulate the antenna effect. We report the synthesis, characterization and photoluminescent properties of Tb-UiO-66 and Tb-UiO-66-$(OH)_2$, as well as three new analogues Tb-UiO-66-F, Tb-UiO-66-Br and Tb-UiO-66-NH_2 (Figure 1), obtained using 2-fluoroterephthalic acid, 2-bromoterephthalic acid and 2-aminoterephthalic acid linkers, respectively.

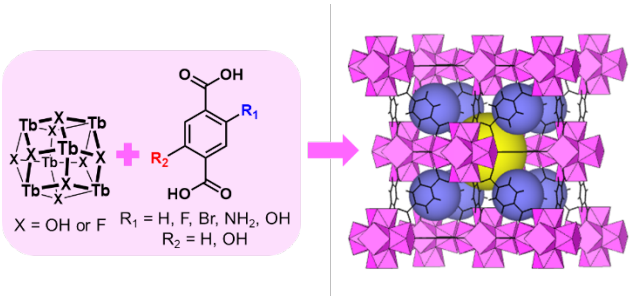

Figure 1 Structure of Tb-UiO-66, the hexanuclear cluster and linkers.

2. EXPERIMENTAL SECTION

2.1 Synthesis of Tb-UiO-66, Tb-UiO-66-F, Tb-UiO-66-Br and Tb-UiO-66-NH$_2$. These Tb-UiO-66 analogues were synthesized through solvothermal synthesis following an adapted procedure reported by our group.[21, 23, 24] They were synthesized in a 6-dram vial by mixing $Tb(NO_3)_3{\cdot}xH_2O$ (79.0 mg, 0.174 mmol, assuming hexahydrate), the corresponding linker, terephthalic acid or a substituted derivative (0.174 mmol), and 2,6-difluorobenzoic acid (2,6-dFBA, 440 mg, 2.78 mmol). The mixture was suspended in *N,N*-dimethylacetamide (DMA, 8 mL) before nitric acid (0.1 mL) and water (0.1 mL) were added. The vial was sealed, sonicated until complete dissolution, and placed in a preheated oven at 120 °C for 24 hours. The solid was separated by centrifugation, washed four times with *N,N*-dimethylformamide (DMF) over 24 hours and four times with acetone over 24 hours. The materials were air-dried, followed by activation at 80°C under vacuum during 20 hours.

2.2 Synthesis of Tb-UiO-66-(OH)$_2$. Tb-UiO-66-(OH)$_2$ was synthesized through solvothermal synthesis by adapting a reported procedure.[27] The sample was synthesized in a 6-dram vial using $Tb(NO_3)_3{\cdot}xH_2O$ (127.3 mg, 0.281 mmol, assuming hexahydrate), 2,5-dihydroxyterepthalic (81.6 mg, 0.412 mmol), and 2-fluorobenzoic acid (2-FBA, 864.0 mg, 6.17 mmol), suspended in DMF (8 mL), MilliQ water (2 mL) and 3.5 M nitric acid in DMF (0.6 mL). The vial was sealed, sonicated and placed in a preheated oven at 120 °C for 72 hours. The precipitate was collected by centrifugation and washed four times with DMF over 48 hours, and four times with acetone over 24 hours. The sample was air-dried before activation at 120 °C under vacuum for 20 hours.

2.3 Characterization. Optical microscopy images were collected using a Laxco LMC-2000 compound microscope system equipped with a SeBaCam digital microscope camera.

Single crystal X-ray diffraction (SCXRD) data was measured on a Bruker D8 Venture diffractometer equipped with a Photon 200 area detector, and *IμS* microfocus X-ray source (Bruker AXS, Cu*K*α source). Measurements were carried out at 298 K. The crystals diffracted weakly at high angles. Structure solutions were carried out using the SHELXTL package from Bruker.[28] The parameters were refined for all data by full-matrix-least-squares or F2 using SHELXL.[29] It should be noted that disordered molecules (water, DMA, and dimethylammonium) in the MOF pores, which could not be reliably modelled using discrete atoms, were subtracted by SQUEEZE, using the PLATON software. All the nonhydrogen atoms were refined with anisotropic thermal parameters. Hydrogen atoms were placed in calculated positions and allowed to ride on the carrier atoms. All hydrogen atom thermal parameters were constrained to ride on the carrier atom.

Powder X-ray diffraction (PXRD) patterns were collected on a Rigaku MiniFlex diffractometer equipped with a Ni-filtered Cu$K\alpha$ X-ray source (λ = 1.54178 Å). The MOF samples were previously dried and packed into a smooth layer on a silicon wafer zero-background sample holder. Results were collected from 5-40° 2θ at 0.02 θ increments in the 2θ-range and a scanning speed of 0.100 °/s.

MOF samples were activated at 80 or 120 °C (as noted above) for 20 hours with the use of a Micromeritics SmartVacPrep instrument equipped with a hybrid turbo vacuum pump. The nitrogen adsorption-desorption isotherms were collected on a Micromeritics Tristar II Plus instrument with an operational nitrogen dewar filled with liquid nitrogen at 77 K.

Scanning electron microscopy (SEM) micrographs were collected on a Phenom ProX desktop SEM. Samples were dispersed on a carbon taped aluminum stub and directly placed on a charge reducing sample holder. SEM images were collected at accelerating voltage of 12 kV and magnification of 1000x.

Proton nuclear magnetic resonance (^{1}H-NMR) spectra were obtained on a 300 MHz Bruker spectrometer. All MOF samples were digested with 8-10 drops of deuterated sulfuric acid (D_2SO_4) followed by sonication and the addition of deuterated dimethyl sulfoxide (DMSO-d_6).

Inductively coupled plasma mass spectrometry (ICP-MS) data were measured with the use of an Agilent 7500 series. Between 1.0-2.0 mg of each Tb-UiO-66 analogue was digested in 0.8 mL HNO_3 by heating the mixture at 100 °C in a sand bath for one hour followed by the addition of 30% H_2O_2. The sample was then placed in a 90 °C sand bath overnight. The solution was diluted with MilliQ water to a final volume of 10 mL and, subsequently, diluted 40 times.

Diffuse reflectance infrared Fourier transform spectroscopy (DRIFTS) spectra were obtained using a Thermo Scientific Nicolet iS50 FTIR spectrometer with an MCT detector with a resolution of 1 cm^{-1} from 4000-650 cm^{-1}. The activated samples were suspended in dry potassium bromide (KBr).

Diffuse Reflectance UV-vis absorption spectroscopy (UV-vis DRS) data were collected using a Cary 5 Series UV-vis-NIR Spectrophotometer (Agilent Technologies) with an EasiDiff™ accessory. Activated MOF samples were loaded into a sample holder with potassium bromide (KBr).

Photoluminescence (PL) spectra and quantum yield (QY) data were collected using a Horiba PTI QuantaMaster 8075 spectrofluorimeter equipped with an integrating sphere. Dry samples were placed between two quartz slides and fixed with grease. The data were collected at an excitation wavelength of 300 nm or 312 nm (for UiO-66-Br) with an integration time of 1 s, step size of 1 nm, slits of 2 nm, and applying a filter at 375 nm.

2.4 Computational methods

All calculations were performed using the Gaussian 09 package suite.[30] The S_0 ground state and the T_1 lowest triplet state of all linkers were optimized at the B3LYP[31, 32]/6-311++G**[33] levels of theory in the gas phase without symmetry constraints. Frequency analysis was performed on the optimized

geometries. Spin-unrestricted calculations were performed on the triplet states. Spin-contamination was found to be negligible in the studied systems. $T_1 \rightarrow S_0$ adiabatic transitions were obtained by calculating ZPE corrected electronic energy for the optimized singlet state and the optimized triplet state. The transition energy was then calculated as the difference between both ZPE corrected electronic energies (ΔSCF method).[34] TD-DFT calculations were also performed on the optimized ground state geometries (S_0) of the linkers to obtain the energies corresponding to vertical $S_0 \rightarrow T_1$ transitions.

3. RESULTS AND DISCUSSION

3.1 Synthesis and characterization. Solvothermal synthetic procedures were used to synthesize the analogues of Tb-UiO-66 reported herein. Tb-UiO-66-F, Tb-UiO-66-Br and Tb-UiO-66-NH_2 were obtained following a reported procedure for Tb-UiO-66.[21, 23, 24] In all cases, $Tb(NO_3)_3{\cdot}xH_2O$ was mixed with the corresponding linker in equimolar ratio, and 2,6-dFBA was used as a modulator. The mixture was dissolved in DMA and nitric acid was added as a co-modulator. Since the addition of water to the reaction has shown to significantly increase the yield,[23] 0.1 mL of water was added in the synthesis of all these Tb-UiO-66 analogues. Tb-UiO-66-$(OH)_2$ was synthesized following a reported procedure.[27] $Tb(NO_3)_3{\cdot}xH_2O$, the DOBDC linker, 2-FBA, and nitric acid were mixed in DMF, and water was also added to the reaction. All samples were washed with DMF and acetone, and then dried in a vacuum oven. The samples dried in the vacuum oven were used to compare to the ones activated at 80°C for 20 hours on the Smart VacPrep instrument, in order to assess the stability of the Tb-UiO-66 analogues to the activation conditions and to determine if activation leads to a difference in the photoluminescence and corresponding quantum yields.

Optical microscopy images were collected upon removal of the sample vials from the oven (Figure S1) and prior to any washing or characterization. The octahedral morphology expected for Tb-UiO-66 is observed for all the analogues. SCXRD data were collected for the analogues: Tb-UiO-66-Br, Tb-UiO-66-F, Tb-UiO-66-NH_2 and Tb-UiO-66-$(OH)_2$ and the crystallographic information is presented in Table S1. The crystal structures were solved in a cubic space group $Fm\bar{3}m$ for Tb-UiO-66,[24] Tb-UiO-66-Br, Tb-UiO-66-F and Tb-UiO-66-NH_2, while the space group for Tb-UiO-66-$(OH)_2$ is found to be $P4/mnc$. In the typical structure described by a cubic crystal system the linker only features the bidentate-bridging coordination geometry. The reason for lower symmetry in Tb-UiO-66-$(OH)_2$ compared to the other MOFs in the series could be explained by a mixture of bidentate-chelate/bidentate-bridging between the linker and the metal centers in the structure, as also observed previously.[27]

The bulk crystallinity as well as the phase purity of all as-synthesized, microcrystalline MOFs was confirmed by comparing the experimental PXRD patterns of all MOFs with the simulated pattern obtained from the single crystal data of Tb-UiO-66, confirming that all MOFs before and after activation are isostructural to Tb-UiO-66 (Figure 2a and 2b). The stability of each MOF after activation was probed by PXRD. The difference in peak intensities observed for some of the samples might be associated with a lack of stability after activation or the generation of smaller crystallites. For Tb-UiO-66-Br, a more prominent decrease in reflection intensity is observed after activation of the MOF, suggesting that Tb-UiO-66-Br is the least stable of all Tb-UiO-66 analogues to activation.

Nitrogen gas adsorption and desorption data were collected for all MOFs (Figure 2c) and type Ia isotherms are observed, which are indicative of microporous materials. This is consistent with the pore size of Tb-UiO-66 being approximately 10 Å.[21] The Brunauer-Emmett-Teller (BET) surface areas are 980, 790, 730, 670 and 600 m^2/g, for Tb-UiO-66, Tb-UiO-66-F, Tb-UiO-66-NH_2, Tb-UiO-66-Br and Tb-UiO-66-$(OH)_2$, respectively, corresponding to what it is expected based on the size and masses of the functional groups on the MOF linkers. A similar surface area is observed for Tb-UiO-66-F and Tb-UiO-66-NH_2 where the size and mass of the functional groups added to the BDC linker do not significantly alter the pore apertures or the molar mass of the MOF. Larger and heavier functional groups such as -Br can obstruct the access to the internal pores of Tb-UiO-66-Br and increase the molar mass of the MOF. Given that surface area here is reported gravimetrically, there is a decreasing trend in surface area as the mass and size of functional groups increases. Tb-UiO-66-$(OH)_2$ exhibits the lowest surface area, which may be explained by the presence of two functional groups on each linker. Additionally, it corresponds well with the previously reported surface area for this MOF.[27]

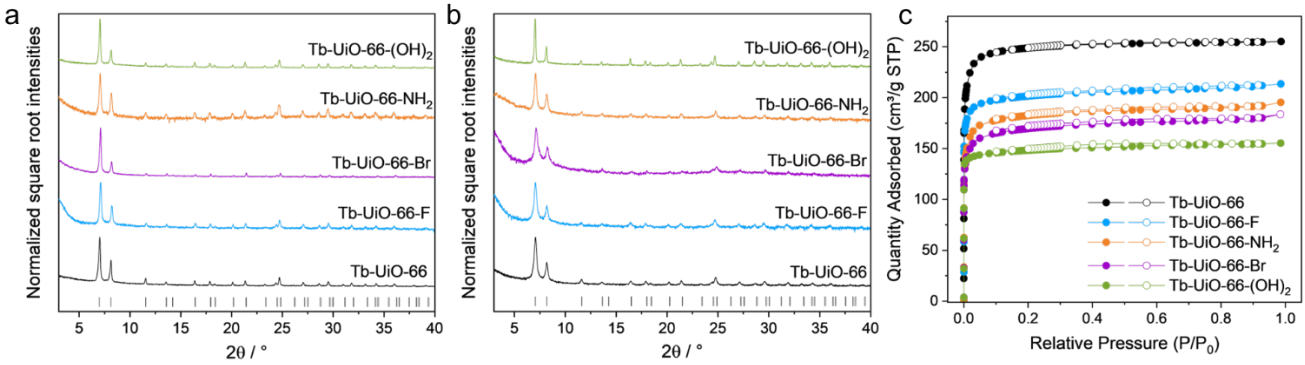

Figure 2 PXRD patterns for the analogues before (a) and after (b) activation and N_2 adsorption-desorption isotherms for all the analogues (c).

The percentage of Tb in each MOF sample was determined by ICP-MS, and in most cases, is in good agreement with the theoretical value calculated for a defect-free MOF (Table S2). In the case of Tb-UiO-66, however, the obtained %Tb is significantly higher (50.76%) than what is expected for a defect-free structure (43.76%). This might be explained by the presence of defects in this MOF. It was previously estimated that one linker might be missing in this structure, with the coordination site on the cluster being capped by acetate ligands which are a product of the decomposition of the DMA solvent, giving a theoretical %Tb of 46-47 %.[23]

SEM micrographs for all analogues were collected after activation (Figure S2). The octahedral morphology for each MOF is observed, which is consistent with the cubic space group of Tb-UiO-66. The particle size varies for the different analogues. Tb-UiO-66 presents the smallest particles with a size under 20 µm, and Tb-UiO-66-$(OH)_2$ exhibits particles with a size above 40 µm, while the other three analogues present intermediate sizes.

^{1}H-NMR spectra of digested samples confirm the presence of the respective linkers in each of the Tb-UiO-66 analogues. The spectrum of Tb-UiO-66 (Figure S3) presents a peak at 7.84 ppm which corresponds to the four equivalent protons of the BDC linker. Additionally, three peaks can be observed at 3.54, 2.80 and 1.94 ppm. These peaks have been assigned to water, possibly from the protonation of the μ_3-OH from the cluster, the counterion, $[(CH_3)_2NH_2]^+$, and acetate ions acting as capping ligands, respectively.[23] The spectrum of Tb-UiO-66-$(OH)_2$ (Figure S4) presents a signal at 7.06 ppm, corresponding to the two equivalent protons of the DOBDC linker. Since Tb-UiO-66-F, Tb-UiO-66-Br and Tb-UiO-66-NH_2 are formed with monosubstituted BDC linkers, three distinct peaks are observed for the aromatic protons (Figure S5, S6 and S7, respectively).

DRIFTS data were collected for the analysis of any IR active functional groups present in all activated Tb-UiO-66 analogues. All the spectra (Figure S8) exhibit a band around 3700 cm^{-1}, corresponding to the stretching of the bridging O–H ligands in the Tb_6-node. For Tb-UiO-66-$(OH)_2$, this stretch is broader due to the additional stretching vibrations of hydroxyl (O–H) groups on the linker. It is possible to observe two C=O stretches from the carbonyl of the carboxylic acid group present at around 1650 and 1400 cm^{-1}, corresponding to the antisymmetric and symmetric modes, respectively. The spectrum of Tb-UiO-66-F presents a band around 1000 cm^{-1}, which can be assigned to the stretching of the C–F bond in the structure of BDC-F. In the spectrum of Tb-UiO-66-NH_2, two bands are observed in the range 3300-3500 cm^{-1}, characteristic of the stretching of the N–H bonds from the primary amine.

The UV-Vis DRS data were collected for all analogues of Tb-UiO-66 as shown in Figure S9. The absorption bands observed were used to select the excitation wavelengths used to collect the photoluminescence spectroscopy data and quantum yields for all MOFs (*vide infra*). The UV-Vis DRS for all the individual linkers was collected (Figure S10) and can be used as a reference for comparison with the absorption spectra of the MOF samples to conclude that there are minimal changes in linker absorption bands after incorporation in the MOF structure.

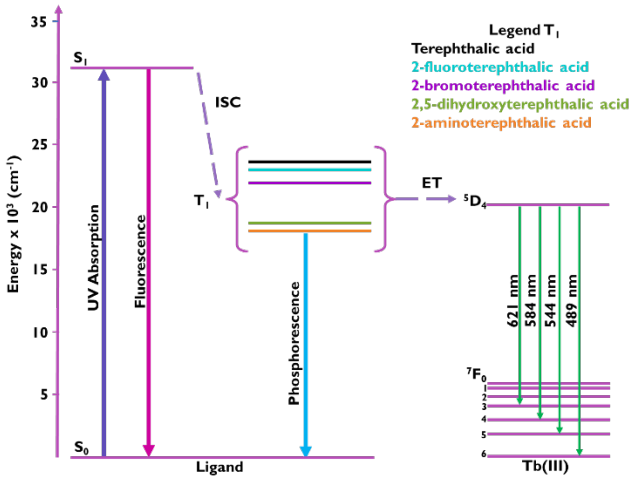

Figure 3 Energy level diagram depicting the T_1 excited energy state for the linkers in the various analogues of Tb-UiO-66, the energy transfer from each linker to Tb(III), and the excited state energies of Tb(III).

3.1 Photoluminescence. The Tb(III) ion emits from a $^5D_4$ state with an energy of 20500 cm^{-1}.[35] Figure 3 depicts the energy level diagram for Tb(III) with a coordinated ligand. On the left, it shows the energy level diagram representing the organic linkers used to synthesize the Tb-UiO-66 analogues and, on the right, the $^5D_4$ state of Tb(III), including the *f-f* transitions that lead to photoluminescence emission. The emission of Tb(III) can be sensitized via the antenna effect. Latva's rule, which is empirically established, states that energy transfer from the organic linker triplet excited state to the $^5D_4$ state of Tb(III) is most efficient when the difference in energy is between 2000-6000 cm^{-1}.[36] If the T_1 energy of the linker is too close to the acceptor state of the lanthanoid, energy back transfer to the linker can occur, leading to partial or complete quenching of the Tb(III) emission. If the T_1 energy of the linker is higher (>6000 cm^{-1} above the emitting state), there will be inefficient energy transfer. Table S3 shows the computational results collected using the B3LYP/6-311++G** model for all the different linkers. The 2-aminoterephthalic acid and 2,5-dihydroxyterephthalic acid linkers have T_1 states lower in energy than the $^5D_4$ state of Tb(III). As such, energy transfer and Tb(III) emission are not expected when excited into these linkers. On the other hand, the three remaining linkers 2-bromoterephtalic acid, 2-fluoroterephthalic, and terephthalic acid are expected to lead to sensitization of Tb(III) according to Latva's rule.

The photoluminescence emission spectrum of Tb-UiO-66-Br is collected by exciting the MOF at 312 nm, while the spectra of all the other analogues are obtained using 300 nm as the excitation wavelength, before and after activation (Figure S11 and 4, respectively). Tb(III) ions emit green with peaks originating from the $^5D_4$ to $^7F_{3,4,5,6}$ transitions typical for Tb(III) at 621, 584, 544 and 489 nm, respectively. These emission bands are observed for Tb-UiO-66, Tb-UiO-66-Br and Tb-UiO-66-F. Tb(III) ion emission is not observed for Tb-UiO-66-NH_2 and Tb-UiO-66-$(OH)_2$, confirming that there is not an efficient energy transfer between the linker and metal, as expected. Some weak BDC linker emission is observed for Tb-UiO-66-Br and

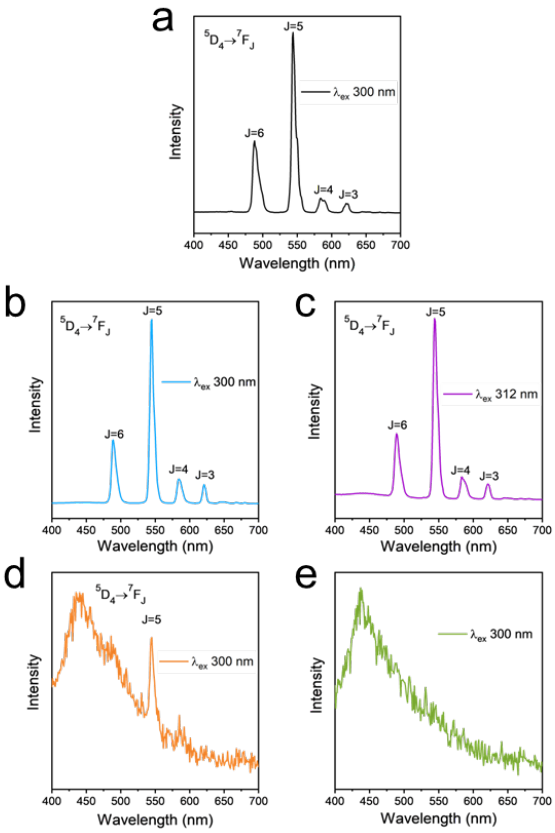

Figure 4 Photoluminescence emission spectra of (a) Tb-UiO-66, (b) Tb-UiO-66-F, (c) Tb-UiO-66-Br, (d) Tb-UiO-66-NH_2, and (e) Tb-UiO-66-$(OH)_2$ after activation.

Tb-UiO-66-F, which is more prevalent before activation, and could be a result of back energy transfer or less efficient forward energy transfer when there are solvent guest molecules in the pores.[37]

Table 1 shows the QY and brightness (B) data that was collected and calculated for all Tb-UiO-66 analogues before and after activation. It is possible to observe similar behavior between QY and B. Relating the QY and the B data shown in Table 1 with the energy level diagram in Figure 3 it is possible to conclude that the linkers BDC, BDC-Br, BDC-F are able to sensitize the emission of the Tb(III) ion. The data collected suggest that BDC and BDC-F are close to the ideal range for an efficient energy transfer to the $^5D_4$ state of Tb(III) since the Tb-UiO-66 analogues synthesized with these linkers show high QYs and B. Tb-UiO-66-Br did not exhibit a high QY nor high B as would be predicted looking at the calculated T_1 energy level of the BDC-Br linker. This unique behavior from Tb-UiO-66-Br may be attributed to the inverse heavy atom effect (HAE) where there is a decrease in spin-orbit coupling upon increasing the atomic number of a chemical element, which can lead to a decrease in photoluminescence.[38]

Although there are very few reported QYs of Tb(III)-MOFs, there are reports of Tb(III)-MOFs with QYs above 90%.[39-41] The QY reported herein for Tb-UiO-66 (25 +/- 2 %) is very similar to that measured for an activated Tb(III)-MOF with metal chain nodes and BDC linkers (26.4+/- 0.3 %).[42] In this previous report by Daiguebonne *et al.* it was found that the hydrated Tb(III)-MOF, $[Tb_2(bdc)_3(H_2O)_4]_n$ presents a higher quantum yield than the dehydrated analogue. Although there is evidence of terminal aqua ligands, with low occupancy, coordinated to the Tb(III) ions in Tb-UiO-66,[24] the degree of hydration of Tb-UiO-66, even before activation, is expected to be much lower than one aqua ligand per Tb(III) ion. This low level of hydration might explain why the QYs of Tb-UiO-66 before and after activation are quite similar, which is different from the trend observed by Daiguebonne and coworkers.

4. CONCLUSION

In summary, the synthesis and characterization of three new analogues of Tb-UiO-66 are reported in this work, using 2-fluoroterephthalic acid, 2-bromoterephthalic acid, and 2-aminoterephthalic acid as linkers to give Tb-UiO-66-F, Tb-UiO-66-Br, and Tb-UiO-66-NH_2, respectively. The photophysical properties of these novel MOFs are compared to those of the reported MOFs, Tb-UiO-66 and Tb-UiO-66-OH_2. The Tb-UiO-66 analogues demonstrate permanent porosity with BET surface areas ranging from 600 to 980 m^2/g. All the linkers used to synthesize these MOFs have different T_1 state energies, leading to differences in the sensitization of Tb(III) photoluminescence, as observed through quantum yield and brightness measurements. Specifically, linker-to-metal energy transfer (or the antenna effect) occurs in Tb-UiO-66, Tb-UiO-66-F, and Tb-UiO-66-Br, leading to green Tb(III) metal-based emission. On the other hand, Tb-UiO-66-NH_2 and Tb-UiO-66-OH_2 do not show any Tb(III) metal-based emission, confirming that linker-to-metal energy transfer does not occur in these MOFs. It is found that the addition of weakly electron withdrawing groups (–F, –Br) on the terephthalic acid linker leads to higher linker T_1 state energies than the addition of electron donating groups.

Table 1 Calculated ΔE (ΔSCF method), QY and Brightness for all the analogues, before and after activation.

Linker	ΔE	QY (%) (before)	SD (%)	QY (%) (after)	SD (%)	Brightness (before)	SD	Brightness (after)	SD
Terephthalic acid	3435	25	1	25	2	0.14	0.04	0.11	0.05
2-fluoroterephthalic acid	3046	31	1	26	2	0.17	0.03	0.12	0.02
2-bromoterephthalic acid	2162	6	2	10	1	0.038	0.016	0.055	0.024
2,5-dihydroxyterephthalic acid	-1334	<1	-	<1	-	0	-	0	-
2-aminoterephthalic acid	-1703	<1	-	<1	-	0	-	0	-

In most cases, the computationally calculated T_1 energy states correlate with the quantum yield and brightness data obtained experimentally, except in the case of Tb-UiO-66-Br, where the inverse heavy atom effect may occur. Overall, the results demonstrate that tuning the functional groups on the terephthalic acid linker of Tb-UiO-66 is a viable strategy for tuning the resulting photoluminescence properties, including QY and B.

ASSOCIATED CONTENT

Optical microscopy and SEM images, crystallographic data tables, ICP analysis, ^{1}H NMR, DRIFTS, UV-Vis, PL spectra, computational results not included in the manuscript and a text file of all computed molecule Cartesian coordinates in a format for convenient visualization can be found in the supporting information.

AUTHOR INFORMATION

Corresponding Author

* ashlee.howarth@concordia.ca

Author Contributions

‖ Ximena A. Canales Gálvez and Micaela Richezzi contributed equally as first author.

The manuscript was written through contributions of all authors. All authors have given approval to the final version of the manuscript.

ACKNOWLEDGMENT

We acknowledge Heng Jiang from the Centre for Biological Applications of Mass Spectrometry at Concordia University for collecting the ICP-MS data. We acknowledge the support of the Natural Sciences and Engineering Research Council of Canada (NSERC), [funding reference number: RGPIN-2018-04388, RGPIN-2024-04293 and ALLRP 570555-2021]. We also acknowledge the support of the Fonds de Recherche du Québec – Nature et Technologies, Établissement de la Relève Professorale: 2020-NC-270099. A.J.H acknowledges the support of the Concordia University Research Chairs Program. N.L. and S.C.P. acknowledge CONICET, Universidad Nacional de Rosario and ANPCyT. We acknowledge the facilities of the CCT-Rosario Computational Center, member of the High Performance Computing National System (SNCAD, MincyT-Argentina), which were used to obtain the presented computational results.

REFERENCES

1. Farha, O. K.; Eryazici, I.; Jeong, N. C.; Hauser, B. G.; Wilmer, C. E.; Sarjeant, A. A.; Snurr, R. Q.; Nguyen, S. T.; Yazaydın, A. O. z. r.; Hupp, J. T., Metal–organic framework materials with ultrahigh surface areas: is the sky the limit? *J. Am. Chem. Soc.* **2012,** *134* (36), 15016-15021.
2. Yaghi, O. M., Reticular chemistry in all dimensions. ACS Publications: 2019; Vol. 5, pp 1295-1300.
3. Batten, S. R.; Champness, N. R.; Chen, X.-M.; Garcia-Martinez, J.; Kitagawa, S.; Öhrström, L.; O'Keeffe, M.; Suh, M. P.; Reedijk, J., Coordination polymers, metal–organic frameworks and the need for terminology guidelines. *CrystEngComm* **2012,** *14* (9), 3001-3004.
4. Batten, S. R.; Champness, N. R.; Chen, X.-M.; Garcia-Martinez, J.; Kitagawa, S.; Öhrström, L.; O'keeffe, M.; Paik Suh, M.; Reedijk, J., Terminology of metal–organic frameworks and coordination polymers (IUPAC Recommendations 2013). *Pure Appl. Chem.* **2013,** *85* (8), 1715-1724.
5. Mason, J. A.; Veenstra, M.; Long, J. R., Evaluating metal–organic frameworks for natural gas storage. *Chem. Sci.* **2014,** *5* (1), 32-51.
6. Wang, C.; An, B.; Lin, W., Metal–organic frameworks in solid–gas phase catalysis. *ACS Catal.* **2018,** *9* (1), 130-146.
7. Otake, K.-i.; Cui, Y.; Buru, C. T.; Li, Z.; Hupp, J. T.; Farha, O. K., Single-atom-based vanadium oxide catalysts supported on metal–organic frameworks: selective alcohol oxidation and structure–activity relationship. *J. Am. Chem. Soc.* **2018,** *140* (28), 8652-8656.
8. Xu, H.; Zhai, B.; Cao, C.-S.; Zhao, B., A bifunctional europium–organic framework with chemical fixation of CO2 and luminescent detection of Al3+. *Inorg. Chem.* **2016,** *55* (19), 9671-9676.
9. Howarth, A. J.; Liu, Y.; Hupp, J. T.; Farha, O. K., Metal–organic frameworks for applications in remediation of oxyanion/cation-contaminated water. *CrystEngComm* **2015,** *17* (38), 7245-7253.
10. Dong, J.; Zhao, D.; Lu, Y.; Sun, W.-Y., Photoluminescent metal–organic frameworks and their application for sensing biomolecules. *J. Mat. Chem. A* **2019,** *7* (40), 22744-22767.
11. Liu, C.; Eliseeva, S. V.; Luo, T.-Y.; Muldoon, P. F.; Petoud, S.; Rosi, N. L., Near infrared excitation and emission in rare earth MOFs via encapsulation of organic dyes. *Chem. Sci.* **2018,** *9* (42), 8099-8102.
12. Cui, Y.; Chen, B.; Qian, G., Lanthanide metal-organic frameworks for luminescent sensing and light-emitting applications. *Coord. Chem. Rev.* **2014,** *273*, 76-86.
13. Xue, D.-X.; Belmabkhout, Y.; Shekhah, O.; Jiang, H.; Adil, K.; Cairns, A. J.; Eddaoudi, M., Tunable rare earth fcu-MOF platform: access to adsorption kinetics driven gas/vapor separations via pore size contraction. *J. Am. Chem. Soc.* **2015,** *137* (15), 5034-5040.
14. Uthappa, U.; Suneetha, M.; Ji, S. M.; Jeong, H.-H.; Han, S. S., Rare earth derived porous metal-organic-frameworks (RE-MOFs) as a smart nanobiomaterials for cancer therapy: Recent trends. *Microporous Mesoporous Mater.* **2023**, 112795.
15. Nguyen, T. N.; Ebrahim, F. M.; Stylianou, K. C., Photoluminescent, upconversion luminescent and nonlinear optical metal-organic frameworks: From fundamental photophysics to potential applications. *Coord. Chem. Rev.* **2018,** *377*, 259-306.
16. Allendorf, M. D.; Bauer, C. A.; Bhakta, R.; Houk, R., Luminescent metal–organic frameworks. *Chem. Soc. Rev.* **2009,** *38* (5), 1330-1352.
17. Bünzli, J.-C. G.; Piguet, C., Taking advantage of luminescent lanthanide ions. *Chem. Soc. Rev.* **2005,** *34* (12), 1048-1077.
18. Wong, K.-L.; Bünzli, J.-C. G.; Tanner, P. A., Quantum yield and brightness. *J. Lumin.* **2020,** *224*, 117256.
19. Amoroso, A. J.; Pope, S. J., Using lanthanide ions in molecular bioimaging. *Chem. Soc. Rev.* **2015,** *44* (14), 4723-4742.
20. Lehn, J. M., Perspectives in supramolecular chemistry—from molecular recognition towards molecular information processing and self-organization. *Angew. Chem. Int. Ed.* **1990,** *29* (11), 1304-1319.
21. Donnarumma, P. R.; Frojmovic, S.; Marino, P.; Bicalho, H. A.; Titi, H. M.; Howarth, A. J., Synthetic approaches for accessing rare-earth analogues of UiO-66. *Chem. Commun.* **2021,** *57* (50), 6121-6124.
22. Vizuet, J. P.; Mortensen, M. L.; Lewis, A. L.; Wunch, M. A.; Firouzi, H. R.; McCandless, G. T.; Balkus Jr, K. J., Fluoro-

Bridged Clusters in Rare-Earth Metal–Organic Frameworks. *J. Am. Chem. Soc.* **2021,** *143* (43), 17995-18000.
23. Richezzi, M.; Donnarumma, P. R.; Copeman, C.; Howarth, A. J., Rare-earth acetates as alternative precursors for rare-earth cluster-based metal–organic frameworks. *Chem. Commun.* **2024,** *60* (39), 5173-5176.
24. Donnarumma, P. R.; Copeman, C.; Richezzi, M.; Sardilli, J.; Titi, H. M.; Howarth, A. J., Deciphering Trends in Structural Parameters of RE-UiO-66 Metal–Organic Frameworks through Single Crystal Analysis. *Cryst. Growth Des.* **2024,** *24* (4), 1619-1625.
25. Ajoyan, Z.; Mandl, G. A.; Donnarumma, P. R.; Quezada-Novoa, V.; Bicalho, H. A.; Titi, H. M.; Capobianco, J. A.; Howarth, A. J., Modulating photo-and radioluminescence in Tb (III) cluster-based metal–organic frameworks. *ACS Mater. Lett.* **2022,** *4* (6), 1025-1031.
26. Ajoyan, Z.; Bicalho, H. A.; Donnarumma, P. R.; Antanovich, A.; Howarth, A. J., Tuning the rare-earth UiO-66 metal–organic framework platform for white light emission. *J. Mat. Chem. C* **2023,** *11* (26), 8929-8934.
27. Sava Gallis, D. F.; Rohwer, L. E.; Rodriguez, M. A.; Barnhart-Dailey, M. C.; Butler, K. S.; Luk, T. S.; Timlin, J. A.; Chapman, K. W., Multifunctional, tunable metal–organic framework materials platform for bioimaging applications. *ACS Appl. Mater. Interfaces* **2017,** *9* (27), 22268-22277.
28. Sheldrick, G. M., SHELXT–Integrated space-group and crystal-structure determination. *Acta Crystallogr. A* **2015,** *71* (1), 3-8.
29. Sheldrick, G. M., Crystal structure refinement with SHELXL. *Acta Crystallogr. C* **2015,** *71* (1), 3-8.
30. Frisch, M. J.; Trucks, G. W.; Schlegel, H. B.; Scuseria, G. E.; Robb, M. A.; Cheeseman, J. R.; Scalmani, G.; Barone, V.; Petersson, G. A.; Nakatsuji, H.; Li, X.; Caricato, M.; Marenich, A. V.; Bloino, J.; Janesko, B. G.; Gomperts, R.; Mennucci, B.; Hratchian, H. P.; Ortiz, J. V.; Izmaylov, A. F.; Sonnenberg, J. L.; Williams; Ding, F.; Lipparini, F.; Egidi, F.; Goings, J.; Peng, B.; Petrone, A.; Henderson, T.; Ranasinghe, D.; Zakrzewski, V. G.; Gao, J.; Rega, N.; Zheng, G.; Liang, W.; Hada, M.; Ehara, M.; Toyota, K.; Fukuda, R.; Hasegawa, J.; Ishida, M.; Nakajima, T.; Honda, Y.; Kitao, O.; Nakai, H.; Vreven, T.; Throssell, K.; Montgomery Jr., J. A.; Peralta, J. E.; Ogliaro, F.; Bearpark, M. J.; Heyd, J. J.; Brothers, E. N.; Kudin, K. N.; Staroverov, V. N.; Keith, T. A.; Kobayashi, R.; Normand, J.; Raghavachari, K.; Rendell, A. P.; Burant, J. C.; Iyengar, S. S.; Tomasi, J.; Cossi, M.; Millam, J. M.; Klene, M.; Adamo, C.; Cammi, R.; Ochterski, J. W.; Martin, R. L.; Morokuma, K.; Farkas, O.; Foresman, J. B.; Fox, D. J. *Gaussian 09 Rev. C.01*, 2016.
31. Becke, A., Thermo chemistry Density-Functional III. The Role of Exact Exchange. *J. Chem. Phys* **1993,** *98* (7), 5648-5652.
32. Stephens, P. J.; Devlin, F. J.; Chabalowski, C. F.; Frisch, M. J., Ab initio calculation of vibrational absorption and circular dichroism spectra using density functional force fields. *J. Phys. Chem.* **1994,** *98* (45), 11623-11627.
33. Hehre, W. J.; Ditchfield, R.; Pople, J. A., Self—consistent molecular orbital methods. XII. Further extensions of Gaussian—type basis sets for use in molecular orbital studies of organic molecules. *J. Chem. Phys.* **1972,** *56* (5), 2257-2261.
34. Guillaumont, D.; Bazin, H.; Benech, J. M.; Boyer, M.; Mathis, G., Luminescent Eu (III) and Gd (III) trisbipyridine cryptates: Experimental and theoretical study of the substituent effects. *ChemPhysChem* **2007,** *8* (3), 480-488.
35. Parker, D., Luminescent lanthanide sensors for pH, pO2 and selected anions. *Coord. Chem. Rev.* **2000,** *205* (1), 109-130.
36. Latva, M.; Takalo, H.; Mukkala, V.-M.; Matachescu, C.; Rodríguez-Ubis, J. C.; Kankare, J., Correlation between the lowest triplet state energy level of the ligand and lanthanide (III) luminescence quantum yield. *J. Lumin.* **1997,** *75* (2), 149-169.
37. Villata, L.; Wolcan, E.; Féliz, M.; Capparelli, A., Solvent quenching of the 5D0→ 7F2 emission of Eu (6, 6, 7, 7, 8, 8, 8-heptafluoro-2, 2-dimethyl-3, 5-octanedionate) 3. *Journal of Photochemistry and Photobiology A: Chemistry* **1998,** *115* (2), 185-189.
38. Havlas, Z.; Michl, J., Prediction of an Inverse Heavy-Atom Effect in H− C− CH2Br: Bromine Substituent as a π Acceptor. *J. Am. Chem. Soc.* **2002,** *124* (20), 5606-5607.
39. Wang, Y.; Yang, X.; Liu, C.; Liu, Z.; Fang, Q.; Bai, F.; Wang, S.; Hou, X.; Feng, B.; Chen, B., Maximized green photoluminescence in Tb-based metal–organic framework via pressure-treated engineering. *Angew. Chem.* **2022,** *134* (48), e202210836.
40. Zhao, Y.; Zhai, X.; Shao, L.; Li, L.; Liu, Y.; Zhang, X.; Liu, J.; Meng, F.; Fu, Y., An ultra-high quantum yield Tb-MOF with phenolic hydroxyl as the recognition group for a highly selective and sensitive detection of Fe 3+. *J. Mat. Chem. C* **2021,** *9* (44), 15840-15847.
41. Meng, D.; Zhao, T.; Busko, D.; Cosgun Ergene, A.; Richards, B. S.; Howard, I. A., Tb and Eu in MOF-76: Elucidating the Mechanisms Responsible for the Divergent Excellent and Poor Photoluminescence Quantum Yields. *Advanced Optical Materials* **2024,** *12* (9), 2300867.
42. Daiguebonne, C.; Kerbellec, N.; Guillou, O.; Bünzli, J.-C.; Gumy, F.; Catala, L.; Mallah, T.; Audebrand, N.; Gérault, Y.; Bernot, K., Structural and luminescent properties of micro-and nanosized particles of lanthanide terephthalate coordination polymers. *Inorg. Chem.* **2008,** *47* (9), 3700-3708.